Peter Cimalla, Theresa Werner, Kai Winkler, Claudia Mueller, Sebastian Wicht, Maria Gaertner, Mirko Mehner, Julia Walther, Bernd Rellinghaus, Dierk Wittig, Mike O. Karl, Marius Ader, Richard H. W. Funk, Edmund Koch

Imaging of nanoparticle-labeled stem cells using magnetomotive optical coherence tomography, laser speckle reflectometry, and light microscopy

Erstveröffentlichung in / First published in:

Journal of Biomedical Optics. 2015 (20), S. 036018-1 – 036018-9 *[Zugriff am: 02.05.2019]*. SPIE Digital Library. ISSN 1560-2281.

DOI: https://doi.org/10.1117/1.JBO.20.3.036018

Journal of Biomedical Optics

BiomedicalOptics.SPIEDigitalLibrary.org

Imaging of nanoparticle-labeled stem cells using magnetomotive optical coherence tomography, laser speckle reflectometry, and light microscopy

Peter Cimalla
Theresa Werner
Kai Winkler
Claudia Mueller
Sebastian Wicht
Maria Gaertner
Mirko Mehner
Julia Walther
Bernd Rellinghaus
Dierk Wittig
Mike O. Karl
Marius Ader
Richard H. W. Funk
Edmund Koch

SPIE.

Journal of Biomedical Optics 20(3), 036018 (March 2015)

Imaging of nanoparticle-labeled stem cells using magnetomotive optical coherence tomography, laser speckle reflectometry, and light microscopy

Peter Cimalla,[a] Theresa Werner,[a] Kai Winkler,[a] Claudia Mueller,[b,c] Sebastian Wicht,[d] Maria Gaertner,[a] Mirko Mehner,[a,e] Julia Walther,[a,e] Bernd Rellinghaus,[d] Dierk Wittig,[b,c] Mike O. Karl,[f,g] Marius Ader,[f] Richard H. W. Funk,[b] and Edmund Koch[a,*]

[a]Technische Universität Dresden, Faculty of Medicine Carl Gustav Carus, Department of Anesthesiology and Intensive Care Medicine, Clinical Sensoring and Monitoring, Fetscherstrasse 74, 01307 Dresden, Germany
[b]Technische Universität Dresden, Institute of Anatomy, Faculty of Medicine Carl Gustav Carus, Fetscherstrasse 74, 01307 Dresden, Germany
[c]Life Science Inkubator GmbH, Ludwig-Erhard-Allee 2, 53175 Bonn, Germany
[d]IFW Dresden, Institute for Metallic Materials, Helmholtzstraße 20, 01069 Dresden, Germany
[e]Technische Universität Dresden, Faculty of Medicine Carl Gustav Carus, Medizinische Physik und Biomedizinische Technik, Fetscherstrasse 74, 01307 Dresden, Germany
[f]Technische Universität Dresden, DFG-Center for Regenerative Therapies Dresden (CRTD), Fetscherstraße 105, 01307 Dresden, Germany
[g]German Center for Neurodegenerative Diseases (DZNE), Arnoldstraße 18, 01307 Dresden, Germany

Abstract. Cell transplantation and stem cell therapy are promising approaches for regenerative medicine and are of interest to researchers and clinicians worldwide. However, currently, no imaging technique that allows three-dimensional *in vivo* inspection of therapeutically administered cells in host tissues is available. Therefore, we investigate magnetomotive optical coherence tomography (MM-OCT) of cells labeled with magnetic particles as a potential noninvasive cell tracking method. We develop magnetomotive imaging of mesenchymal stem cells for future cell therapy monitoring. Cells were labeled with fluorescent iron oxide nanoparticles, embedded in tissue-mimicking agar scaffolds, and imaged using a microscope setup with an integrated MM-OCT probe. Magnetic particle-induced motion in response to a pulsed magnetic field of 0.2 T was successfully detected by OCT speckle variance analysis, and cross-sectional and volumetric OCT scans with highlighted labeled cells were obtained. In parallel, fluorescence microscopy and laser speckle reflectometry were applied as two-dimensional reference modalities to image particle distribution and magnetically induced motion inside the sample, respectively. All three optical imaging modalities were in good agreement with each other. Thus, magnetomotive imaging using iron oxide nanoparticles as cellular contrast agents is a potential technique for enhanced visualization of selected cells in OCT. [DOI: 10.1117/1.JBO.20.3.036018]

Keywords: regenerative medicine; optical coherence tomography; cell imaging; magnetic nanoparticles; stem cells; laser speckle.

Paper 140823PR received Dec. 12, 2014; accepted for publication Mar. 12, 2015; published online Mar. 30, 2015.

1 Introduction

Regenerative medicine is a clinical reality for many organs and tissues and yet a promising research area for neurodegenerative diseases. Focusing on the eye, retinal neurodegenerations caused by age-related macular degeneration and hereditary retinal disorders such as retinitis pigmentosa represent leading causes of visual impairment and blindness in the industrialized countries[1] with no curative therapies available yet. Nowadays, an increased knowledge of the underlying disease mechanisms has initiated the development of novel therapeutic strategies including cell-based approaches. Recent studies in animal models provided proof-of-principle evidence for cell transplantation as a potential future treatment option for retinal neurodegenerations.[2,3] In this situation, donor cells are transplanted into the eye in order to protect or replace degenerating photoreceptors or retinal pigment epithelium (RPE).

However, currently, no three-dimensional (3-D) imaging technique is available that would allow the follow-up of transplanted donor cells and track their fates, i.e., migration and integration, in the host tissue under *in vivo* conditions. To overcome this lack of technology, we suggest cell labeling prior to transplantation with biocompatible contrast agents such as functionalized nanoparticles. Due to its contactless volumetric imaging capability, high acquisition speed, and potential cellular resolution, optical coherence tomography (OCT) is a highly promising approach for *in vivo* retinal cell tracking. However, OCT is a rather unspecific imaging modality that provides only general morphologic information based on light scattering at cells and cellular components such as nuclei and mitochondria. As a consequence, contrast agents are required to enhance visualization of specific cells in tissue.

Among others, magnetic micro- and nanoparticles were proposed as such contrast agents for magnetomotive OCT (MM-OCT), in which they are excited into motion by a modulated external magnetic field.[4,5] By quantification of the elastic tissue displacement in the particle vicinity, MM-OCT contrast enhancement with single cell resolution can be achieved.[6] In addition to pure magnetic particles, fluorescent magnetic

*Address all correspondence to: Edmund Koch, E-mail: edmund.koch@tu-dresden.de

1083-3668/2015/$25.00 © 2015 SPIE

nanoparticles with functionalized coatings also became available recently. Due to their capability of biomolecule coupling, these particles are easily taken up by cells via endocytosis.[7] Hence, using the particles' fluorescent and magnetic properties, they were successfully applied to observe *in vivo* cell tracking by the presence of fluorescence and magnetic resonance imaging (MRI) detection in target tissues or organs.[8] In this work, fluorescent magnetic particles also have been applied for biomechanical experiments at the single cell level using multiphoton microscopy and MM-OCT.[9,10]

However, all MM-OCT methods presented on cell imaging suffer from two major drawbacks. First, detection of magnetically labeled cells in a tissue-like environment was demonstrated exclusively on macrophages[6,11] and platelets,[12,13] which have the ability to internalize large amounts of magnetic particles—a feature that cannot necessarily be observed in other cell types. Second, magnetomotive imaging is restricted to thin samples either due to a short working distance of the solenoid, which is typically 1 to 2 mm in single-sided devices,[14] or because of the limited space in double-sided setups, at which the imaging system and the solenoid are located above and underneath the sample, respectively.[9–11]

In this work, we provide evidence for MM-OCT imaging of single cells that are not macrophages or platelets but are mesenchymal stem cells (MSCs). In the field of regenerative medicine, MSCs are used as potential cell therapy candidates for treatment of ocular diseases.[15–18] These cells were labeled with fluorescent iron oxide nanoparticles that allow parallel detection by means of fluorescence. Furthermore, we use a novel single-sided MM-OCT device with a large working distance of 6 mm as a potential probe for future cell tracking in the mouse retina. Additionally, using light microscopy and laser speckle reflectometry, we investigate the multimodal contrast capability of the applied cellular nanoprobes.

2 Methodology

2.1 *Magnetomotive Optical Coherence Tomography Setup*

All experiments were carried out with a self-developed spectral-domain OCT system operating at 880 nm, which is described in more detail elsewhere.[19] In brief, the system is equipped with a superluminescent diode (Exalos EXS8810-2411, Switzerland) with a center wavelength of 876 nm and a bandwidth of 64 nm full width at half maximum. Interference spectra are generated in a separate fiber-coupled OCT scanning unit containing a Michelson interferometer and are subsequently detected using a linear-in-wavenumber spectrometer and a charge-coupled device (CCD) line scan sensor (Teledyne DALSA IL–C6–2048C, Canada) with a high dynamic range of 80 dB. The CCD line acquisition rate has a fixed value of 11.9 kHz, which is defined by the custom-made readout electronics. Each acquired line scan, i.e., interference spectrum, is converted into an axial depth scan (A-scan) giving the reflectance profile of the sample. Typically, a series of 480 adjacent A-scans are then laterally combined to create a cross-sectional tomographic image (B-scan). The OCT system provides an axial resolution of 6 μm in air, an optical imaging depth of 3 mm, and a sensitivity of −102 dB.

In order to generate a magnetic field for magnetomotive imaging, an electromagnet (Intertec Components ITS-MS 5030 12 VDC, Germany) was integrated into the OCT scanning unit. The optics of the scanning unit was partially incorporated into a center bore of the solenoid's ferromagnetic core in order to optimize working distance. To maximize the amount of core material and thus the magnetic field, a small bore size was chosen suitable to bear 0.25-in. optics. In summary, this MM-OCT probe has a working distance of 6 mm measured from the solenoid surface, an imaging numerical aperture (NA) of 0.1, and a field of view of 1.5 mm in diameter in the focal plane.

The solenoid coil (18.5 Ω) is driven in a pulsed operation mode as proposed by Koo et al.[11] by a self-developed capacitive-discharge pulse generator that is synchronized to the OCT system. To that, a power capacitor (Vishay BCcomponents MAL210222472E3) of 4.2 mF is charged by a dc power supply with up to 120 V. Once the charging is completed, the capacitor is grounded using an insulated-gate bipolar transistor switch (IXYS Corporation IXGH48N60C3), and the resulting high discharge current is conducted through the coil. As shown in Figs. 1(a) and 1(b), a peak current of 5.7 A was obtained with this setup, which resulted in a maximum magnetic flux density of 0.2 T (measured with Magnetometer KOSHAVA 5, Wuntronic GmbH, Germany) and an axial field gradient of 18 T/m at a working distance of 6 mm. The magnetic pulse length related to the 90% level of the pulse maximum was measured to be 33 ms, which is in the range of the B-scan period (40 ms) of the OCT system. Typically, the magnetic field is switched on for 80 ms, (two B-scans), as depicted in Fig. 1(a), with a repetition rate of 1 Hz. During the pulse, the magnetic flux density peaks within 10 ms after current onset and falls off to approximately 71% of its maximum value at current shut-down. The corresponding time period of 0.92 s between adjacent pulses is thereby used to recharge the capacitor. Due to this relatively small duty cycle of 8%, no additional cooling of the solenoid is required.

2.2 *Magnetic Nanoparticles and Magnetic Forces*

For the magnetic labeling of cells, commercially available nanoparticles (nano-screenMAG/R-DXS, chemicell, Germany) were used. These particles exhibit a distinct core-shell structure, where the core is formed through the agglomeration of magnetite (Fe_3O_4) primary particles with sizes in the range of 8 to 12 nm. Each core is surrounded by a fluorescent shell and a coating of dextran sulfate for biomolecule coupling. The hydrodynamic diameter of the particles amounts to 200 nm, while the core size is roughly 170 nm (personal communication with manufacturer). The fluorescence excitation and emission maximum of the selected nanoparticles were in the green and red visible spectral ranges (578 nm/613 nm), respectively.

The particle structure and morphology were characterized by means of transmission electron microscopy (TEM) using a FEI Tecnai 20 microscope with a thermal LaB_6 emitter at an accelerating voltage of 200 kV. Our structural investigations confirmed the information provided by the manufacturer. As an example, a TEM overview image of the particles dispersed on an amorphous carbon support film is shown in Fig. 1(c).

The magnetic properties of the particles were measured by vibrating sample magnetometry using a physical property measurement system (PPMS, Quantum Design). The magnetization curve shown in Fig. 1(d) was obtained from a macroscopic ensemble of particles at room temperature in a magnetic field of up to 3 T. The magnetization loop is hysteretic with coercive fields of roughly 20 mT and a slow approach to saturation below 1 T. This reveals that the particles are ferromagnetically blocked,

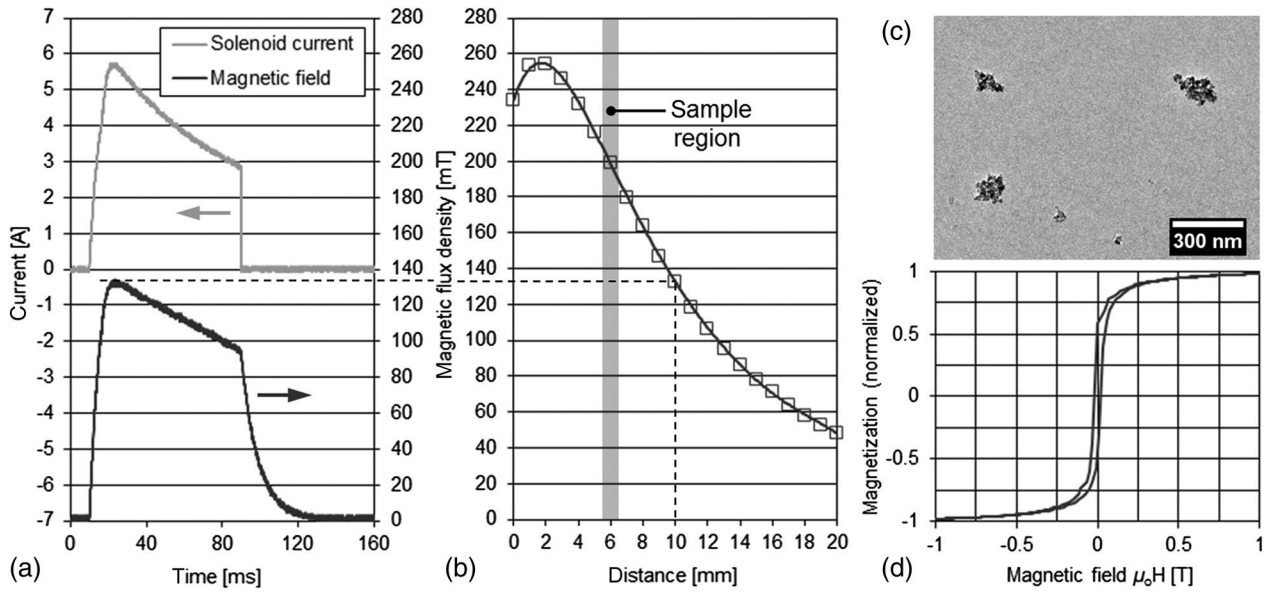

Fig. 1 Pulsed magnetic field and magnetic nanoparticles: (a) Current pulse using a capacitor charging voltage of 120 V and resulting magnetic flux density measured 10 mm above the solenoid's surface. (b) Peak magnetic flux density versus axial distance from solenoid. (c) Electron microscopy image and (d) magnetization curve of the applied magnetic nanoparticles.

which is consistent with the size of the magnetic core. While individual magnetite particles are expected to be superparamagnetic at sizes below 26 nm, the agglomeration of primary particles to a larger magnetic entity (with a diameter of 170 nm) leads to an increase of the superparamagnetic blocking temperature to beyond their Curie temperature. Hence, the particles respond as "normal" blocked ferromagnets.

In order to obtain a large magnetomotive effect that can be detected with sufficient signal-to-noise ratio, a high magnetic force is desired. To illustrate the fundamental relation between the magnetic field and the force, we approximate the slightly ferromagnetic particles (small hysteresis and low remanent magnetization) by paramagnets. Hence, the magnetic force F_z that attracts the particles at location r in the axial direction (z-direction) toward the solenoid can be expressed by Eq. (1):

$$F_z(r) = \frac{V_p \cdot (\chi_p - \chi_m)}{\mu_0} \cdot B(r) \cdot \frac{\partial B(r)}{\partial z}, \tag{1}$$

where V_p is the particle volume, χ_p and χ_m are the magnetic susceptibilities of the particles and the surrounding medium, respectively, μ_0 is the magnetic field constant, B is the magnetic flux density, and $\partial B/\partial z$ is the derivative of B in the z-direction. If the current through the solenoid coil is varied, $\partial B/\partial z$ changes accordingly to B, and the magnetic force F_z scales with B to the power of 2, as long as the particles are not magnetically saturated

$$F_z \propto B^2 | B < B_{\text{saturation}}. \tag{2}$$

Hence, in this nonsaturation regime, F_z can be enhanced relatively easily, since a twofold increase of the solenoid current, i.e., magnetic flux density, would result in a fourfold magnetic force.

In saturation, however, the particle magnetization $\chi_p B/\mu_0$ in Eq. (1) becomes a constant value, which cannot be further increased by the magnetic field. Hence, neglecting the small magnetization of the diamagnetic medium, the magnetic force increases only with $\partial B/\partial z$, i.e., F_z scales with B to the power of 1:

$$F_z \propto B | B \geq B_{\text{saturation}}, \tag{3}$$

for flux densities equal to or larger than $B_{\text{saturation}}$.

As it can be seen in the magnetization curve in Fig. 1(d), saturation of the particles is already beginning at approximately 0.1 T, whereas the maximum flux density delivered by the solenoid was measured to be 0.2 T in the sample region. Therefore, we assume that further increase of the flux density would have only a reduced effect on the magnetic force due to operation in the saturation regime. Moreover, the generation of stronger magnetic fields is technically challenging since the solenoid's efficiency significantly degrades at higher currents due to the limited permeability (saturation) of the ferromagnetic core. Considering these facts and taking into account that the present field parameters ($B = 0.2$ T and $\partial B/\partial z = 18$ T/m) are slightly above the values reported for *in vivo* MM-OCT studies,[20] no additional efforts were made to further increase the magnetic field.

2.3 *Light Microscopy and Laser Speckle Reflectometry*

In order to investigate the MM-OCT signal in dependency of the cellular magnetic particle content, combined OCT and light microscopy imaging of identical cells are necessary. Therefore, we integrated the MM-OCT probe into a conventional epi-fluorescence microscope (Leica DMRB, Germany) by replacing the microscope's condenser unit. As shown in Fig. 2, the OCT scanning unit was positioned upside-down in a way that the distal end of the probe with the solenoid and the OCT objective lens is placed directly underneath the object stage of the microscope. With this setup, it is possible to image the same cells with both two-dimensional (2-D) light microscopy (bright-field/multicolor

fluorescence) and 3-D OCT in an upright and an inverted configuration, respectively.

In addition to MM-OCT and light microscopy, we use laser speckle reflectometry as a 2-D reference modality to investigate sample motion.[21] To that, the sample was illuminated in a dark-field manner by a collimated laser beam at 638 nm, which was generated by a fiber-coupled laser diode with 1 mW output power (Lasiris PTL-500-635-1-2.0, Coherent Canada) and a fiber collimator (Fig. 2). The collimator was mounted on a post next to the microscope using tip/tilt kinematics to adjust the laser beam to the microscope's field of view. The diameter of the collimated beam was approximately 4 mm and the incident angle between the laser beam and the sample surface was approximately 35 deg. Due to the spatial coherence of the illuminating laser, a speckle pattern is created throughout the observed sample, which was detected using the microscope's video camera (1.3 megapixel monochrome CMOS, Sumix SMX-M71M). The speckle pattern depends on the distribution and distance of single scatterers relative to each other. Hence, local distance changes due to moving scatterers result in an altered speckle pattern in the area around the magnetic nanoparticles. Therefore, motion contrast with subwavelength sensitivity can be achieved by calculating the intensity variance of the raw speckle images over time.

2.4 *Signal Processing*

To retrieve magnetomotive contrast from the acquired image data, the following signal processing was applied. In laser speckle reflectometry, raw speckle images were recorded in the presence of the pulsed magnetic field and the laser speckle variance (LSV) σ^2_{LS} was calculated in a sliding window manner over five adjacent video frames, as indicated in Eq. (4):

$$\sigma^2_{\mathrm{LS}} = \frac{1}{n-1}\sum_{i=0}^{n-1}(I_i - I_{\mathrm{mean}})^2 \Big| n = 5, \tag{4}$$

where I_i is the pixel intensity in the i'th image and I_{mean} is the average pixel intensity of the frame interval. Afterward, a Gaussian convolution filter with a kernel size of 7×7 pixels was applied to smooth variance images and to suppress noise.

Magnetomotive contrast in OCT was obtained similar to laser speckle reflectometry by OCT speckle variance analysis. To that, the variance σ^2_{OCT} of the OCT signal amplitude in linear scale was calculated over five adjacent B-scans, as indicated in Eq. (5):

$$\sigma^2_{\mathrm{OCT}} = \frac{1}{n-1}\sum_{i=0}^{n-1}(A_i - A_{\mathrm{mean}})^2 \Big| n = 5, \tag{5}$$

where A_i is the linear, nonsquared OCT signal amplitude for each pixel of the i'th B-scan and A_{mean} is the average amplitude for each pixel in the B-scan interval. The resulting variance image was then smoothed with a Gaussian convolution filter of 3×3 pixels and converted to the logarithmic dB-scale, as in Eq. (6):

$$\sigma^2_{\mathrm{OCT}}/\mathrm{dB} = 10 \cdot \lg(\sigma^2_{\mathrm{OCT}}), \tag{6}$$

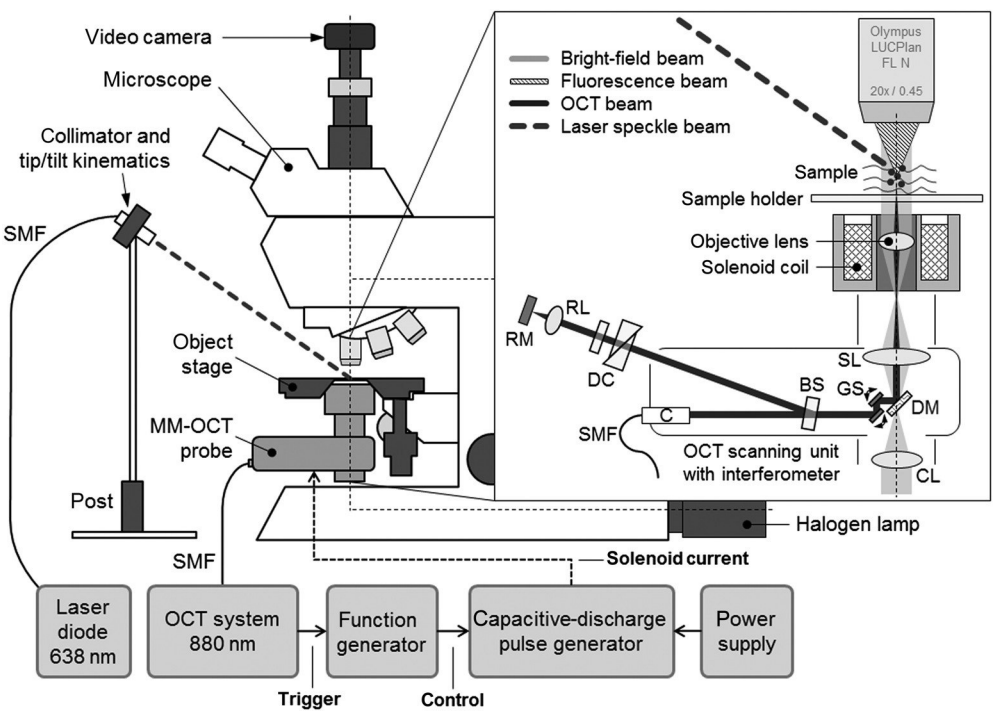

Fig. 2 Setup for combined magnetomotive optical coherence tomography (MM-OCT), laser speckle reflectometry, and light microscopy. The microscope is equipped with a halogen lamp for bright-field transmission imaging and a mercury-vapor lamp (not shown) for epifluorescence imaging. The inset shows a detailed view of the sample region and the OCT scanning unit with attached electromagnet. Abbreviations: BS—beam splitter, C—collimator, CL—condensing lens, DC—dispersion compensation, DM—Vis/NIR dichroic mirror, GS—galvanometer scanners, RL—reference lens, RM—reference mirror, SL—scanning lens, and SMF—single-mode fiber.

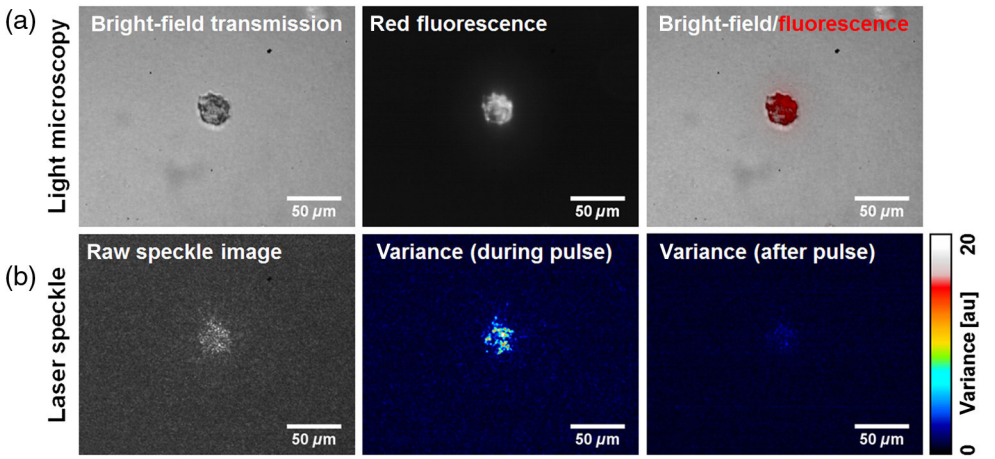

Fig. 3 (a) Light microscopy and (b) laser speckle reflectometry of a single mesenchymal stem cell (MSC) labeled with fluorescent magnetic nanoparticles and embedded in 1% agar.

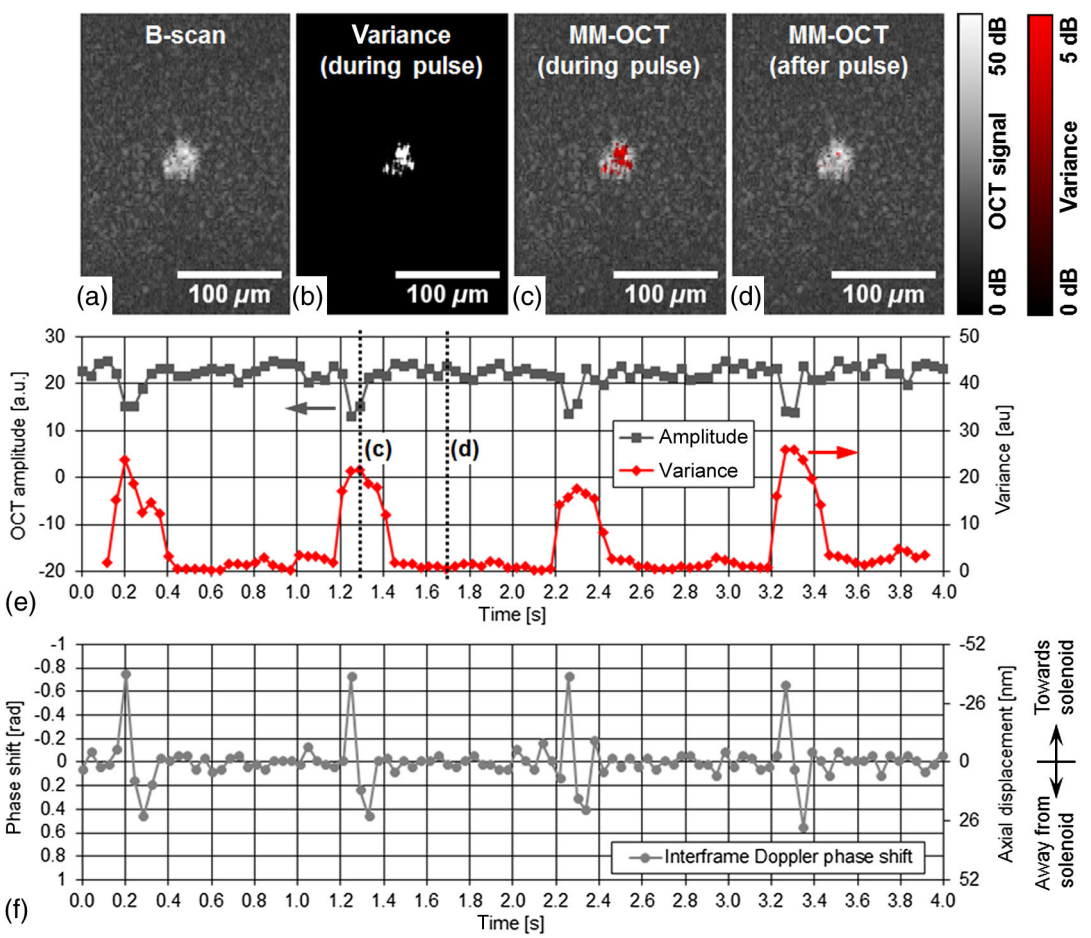

Fig. 4 MM-OCT imaging of a single MSC in 1% agar: (a) OCT cross-section (average of five B-scans) of the same cell as shown in Fig. 3. (b) Variance image calculated over five adjacent B-scans during the magnetic pulse. (c) Color-encoded MM-OCT image [overlay of (a) and (b)] during the pulse and (d) after the pulse. (e) Time course of the OCT signal amplitude and temporal variance in a linear scale for one image pixel inside the cell. The positions of the MM-OCT images during and after the pulse (c and d) are marked by the dotted lines. (f) The corresponding interframe Doppler phase shift of the OCT signal indicates alternating particle motion toward and away from the solenoid in the nanometer scale. In both (e) and (f), the pulse repetition rate of 1 Hz can clearly be identified.

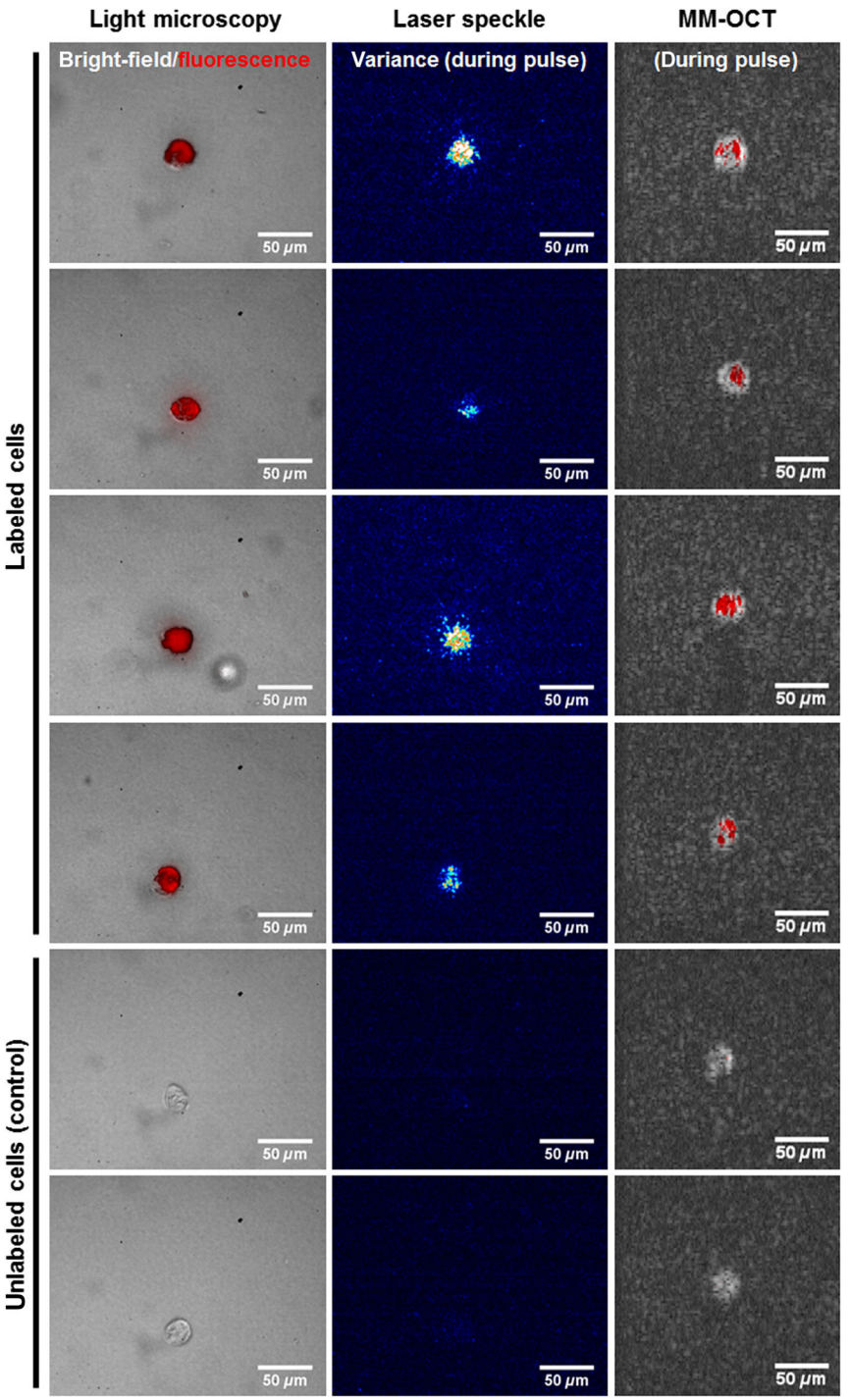

Fig. 5 Multimodal imaging of MSCs in tissue-mimicking agar scaffolds. The labeled cells (upper four rows) are characterized by an intense red fluorescence signal in the microscopy images and a significantly increased variance in both the laser speckle images and the MM-OCT cross-sections, which is caused by magnetically induced motion. In contrast, the unlabeled control cells (lower two rows) show no fluorescence and no motion. The color and brightness scale of the laser speckle variance (LSV) and MM-OCT images are identical to Figs. 3 and 4, respectively.

in order to improve visibility of small values. Finally, the motion information of the OCT variance image was color-encoded and overlaid on the structural information of the conventional B-scan to generate the MM-OCT image. To that, a color image in the hue-saturation-value space was created and the variance and structural images were plotted in the saturation and value channel, respectively, while the hue channel was set to a constant value of zero, which corresponds to red color.

Moreover, phase-resolved Doppler OCT[22] was applied to estimate the magnitude of particle motion. To that, the Doppler phase shift between OCT signals of adjacent B-scans (interframe Doppler OCT) was analyzed to retrieve the axial displacement

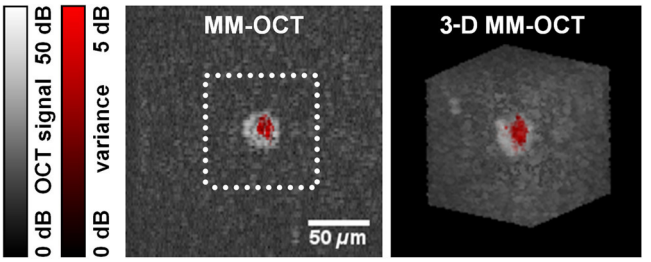

Fig. 6 Cross-sectional and three-dimensional (3-D) MM-OCT image (maximum intensity projection) of a labeled MSC. The dotted square denotes the region of the depicted 3-D data.

of the sample in response to the magnetic pulse. The relation between the axial displacement Δz and the measured Doppler phase shift $\Delta\varphi$ is given by Eq. (7):

$$\Delta z = \frac{\Delta\varphi \cdot \lambda_0}{4\pi \cdot n}, \tag{7}$$

where λ_0 is the center wavelength of the OCT system (876 nm) and n is the refractive index of the sample (1.33 for water). In this work, the sign of the phase shift implies the direction of the axial displacement, i.e., negative and positive values correspond to particle motion toward and away from the solenoid, respectively, as long as no phase-wrapping occurs.

2.5 *Sample Preparation and Elasticity Estimation*

Magnetic cell labeling and sample preparation for cell experiments were performed as follows: MSCs were seeded on a cell culture dish and cocultured with nanoparticle solution (0.5 mg/ml) for 24 h. After rinsing with phosphate-buffered saline (PBS), adherent MSCs were detached from the dish using trypsin and resuspended in fresh cell culture medium. Finally, MSCs were embedded in tissue-mimicking scaffolds made of 1% agar, 49% PBS, and 50% cell culture medium, similar to the protocol proposed by Oldenburg et al.[6] Molded agar-cell samples with a thickness of 3 to 4 mm were then created in 40-mm cell culture dishes and kept at resting conditions for solidification. Control samples with unlabeled cells were created identically, except that MSCs were not cocultured with magnetic nanoparticles. In terms of cellular particle concentration and its effect on cell function, recent literature indicates that MSCs incubated with 200-nm magnetic particles coated with dextran sulfate take up ~10 pg of iron oxide per cell and show a cell viability of ~70% after 24 h.[23]

To estimate the elasticity of the agar scaffold, we applied the principles of contact mechanics. To that, a small steel ball (diameter: 3.16 mm and weight: 130 mg) was placed on top of a thick 1% agar sample, which led to an indentation of the elastic surface at the contact point. Following the Hertz model in Eq. (8)

$$F = \frac{4 \cdot E}{3 \cdot (1-\nu^2)} \cdot R^{1/2} \cdot d^{3/2}, \tag{8}$$

the Young's modulus E of the sample can then be calculated from the known weight force F and radius R of the steel ball, the corresponding indentation d, and the Poisson's ratio ν of the soft material. Since ν is often not exactly known, the apparent elastic modulus K given by Eq. (9)

$$K = \frac{E}{1-\nu^2}, \tag{9}$$

is used instead to describe the sample elasticity. Hence, using Eqs. (8) and (9), K can be easily retrieved by registering the indentation, which was achieved by cross-sectional OCT imaging of the sample surface with and without steel ball load. With this method, the apparent elastic modulus of 1% agar gel was measured to be ~0.5 kPa, which is slightly lower but comparable with the values of 0.9 to 1.8 kPa given for the retina.[24] We, therefore, chose to keep the 1% agar gel as the tissue-mimicking scaffold in order to make our experiments comparable with the work of Oldenburg et al.[6]

3 Cell Imaging

In order to investigate nanoparticle contrast enhancement, we carried out *in vitro* experiments in which we use MM-OCT, laser speckle reflectometry, and light microscopy to image single cells in a 3-D, tissue-like environment. To that, agar samples with embedded MSCs were prepared as described in Sec. 2.5 and placed on the microscope object stage (Fig. 2) for multimodal imaging. As shown in Fig. 3, single cells in the sample volume were localized by bright-field microscopy using a 20× long-working distance objective with an NA of 0.45 (Olympus LUCPlanFL N). Cell labeling with nanoparticles was validated by using the red fluorescence channel of the microscope. A potential agglomeration of the magnetically labeled cells due to the slightly ferromagnetic particles was not observed. Furthermore, laser speckle images were recorded and LSV was calculated as described in Sec. 2.4. As it can be seen in Fig. 3, a significant increase of the LSV signal occurs in the cell region when the magnetic pulse is active. Hence, cellular magnetomotion can be assumed.

After microscopy and laser speckle reflectometry, the same cells were imaged with OCT under the influence of the pulsed magnetic field. Proper alignment of the modalities was achieved by imaging the scanning OCT beam with the microscope camera. The OCT imaging parameters were set to 480 A-scans per B-scan, whereas the first 32 A-scans of each frame were used for calibration purposes and are not part of the true cross-sectional B-scan image. The step size was set to 0.5 μm to achieve dense sampling of the small cellular structures. At least 25 B-scans covering a time period of 1.008 s were recorded at one position in order to acquire a complete magnetic pulse cycle. As shown in Figs. 4(a)–4(e), magnetomotive contrast in the OCT cross-sectional images of the cells was then obtained similar to laser speckle reflectometry by OCT speckle variance analysis, as described in Sec. 2.4. It can be seen that the OCT speckle variance inside the cell is also significantly increased during the magnetic pulse, which leads to a substantial depth-resolved color contrast in the MM-OCT image. Moreover, as indicated in Fig. 4(f), interframe Doppler OCT analysis revealed plausible particle motion toward and away from the solenoid when the current is switched on and off, respectively. The corresponding axial particle displacement was measured to be in the range of 40 nm.

Further cell imaging examples are depicted in Fig. 5. There, it can be seen that the labeled cells are always characterized by an intense red fluorescence signal and a significant LSV and MM-OCT motion contrast as a result of the fluorescent and magnetic properties of the applied nanoparticles. Compared with that, the unlabeled control cells show no fluorescence and

no magnetomotion, neither in LSV nor in MM-OCT. Hence, all three modalities are in good agreement with each other and allow distinguishing labeled cells from unlabeled ones. However, MM-OCT is the only imaging technique that enables depth-resolved contrast and 3-D visualization of labeled cells, as shown in Fig. 6. This 3-D MM-OCT dataset was obtained by recording a volume scan consisting of 1000 B-scans acquired in brightness-motion mode, i.e., 25 B-scans (one magnetic pulse cycle) were recorded at the same location using the fast scanning axis before the galvanometer scanner of the slow scanning axis was set one step further. The step size of the slow axis was set to 2.3 μm, which resulted in a scanned area of 224 μm $\times$ 92 μm (fast axis $\times$ slow axis) on the sample. The acquisition time of the 3-D MM-OCT dataset was 40.3 s.

4 Discussion and Conclusion

In conclusion, our results show that the magnetomotive imaging in combination with iron oxide nanoparticles as cellular contrast agents is a suitable method to enhance visibility of specific cells in OCT. These findings are encouraging for further development toward noninvasive 3-D cell tracking in the retina and other target tissues. In this work, we were able to make some important contributions toward this final goal. To the best of our knowledge, we present for the first time MM-OCT imaging of single MSCs, which are potential cell therapy candidates in regenerative medicine. Furthermore, we developed a single-sided MM-OCT probe with a relatively large working distance of 6 mm, which facilitates future use for *in vivo* retina imaging in experimental mouse models (eye length ~3 mm). In general, the MM-OCT method presented in this work is intended for research purposes in animal models only. It is not recommended for MRI studies because the slightly ferromagnetic particles might produce heat in the oscillating magnetic field. Currently, in the state of *in vitro* experiments, the developed MM-OCT probe can also be integrated into a conventional microscope, which is very useful for parallel reference imaging of the investigated cells.

Regarding cell motion, no displacement or deformation of the MSCs was visible during the presence of the pulsed magnetic field, neither in OCT nor in light microscopy. Because of the fact that the color-coded speckle variance signals of both MM-OCT and laser speckle reflectometry do not cover the entire cells (Figs. 4 and 5), it is reasonable to conclude that the cells do not move as a whole, but that the magnetically induced motion is limited to the intracellular space. In terms of motion magnitude, particle displacements of ~40 nm, as measured by Doppler OCT, seem to be sufficient to cause the observed laser speckle and OCT speckle effects. This dislocation is below the size of small cell organelles such as vesicles and mitochondria, and therefore, should not be harmful to the cell's mechanical integrity. However, further investigations about cell viability after magnetomotive imaging and nanoparticle labeling of other cell types relevant for therapeutic transplantation approaches, such as photoreceptor precursors and RPE cells, are necessary to establish the method. Further, the reduced cell viability that is indicated in the literature for the use of dextran sulfate-coated particles could be improved by using particles coated with starch.[23]

Moreover, for future *in vivo* application, faster imaging is desired. Currently, the magnetomotive imaging speed is limited by the pulse repetition rate of 1 Hz. Further increase of the pulse rate, i.e., decrease of the capacitor charging time, by means of an adequate power supply is subject of current investigation. Alternatively, a sinusoidal magnetic waveform permits shorter imaging times, too, however, it requires sophisticated cooling of the solenoid due to the higher power consumption compared with pulsed operation.

Acknowledgments

This research was supported by the TU Dresden CRTD (Center for Regenerative Therapies Dresden) Seed Grant Program and grants from the MeDDrive program of the Faculty of Medicine Carl Gustav Carus of the TU Dresden.

References

1. C. Bunce and R. Wormald, "Leading causes of certification for blindness and partial sight in England & Wales," *BMC Public Health* **6**(1), 58 (2006).
2. U. Bartsch et al., "Retinal cells integrate into the outer nuclear layer and differentiate into mature photoreceptors after subretinal transplantation into adult mice," *Exp. Eye Res.* **86**(4), 691–700 (2008).
3. M. Carido et al., "Characterization of a mouse model with complete RPE loss and its use for RPE cell transplantation," *Invest. Ophthalmol. Visual Sci.* **55**(8), 5431–5444 (2014).
4. A. Oldenburg et al., "Magnetomotive contrast for *in vivo* optical coherence tomography," *Opt. Express* **13**(17), 6597–6614 (2005).
5. A. L. Oldenburg et al., "Phase-resolved magnetomotive OCT for imaging nanomolar concentrations of magnetic nanoparticles in tissues," *Opt. Express* **16**(15), 11525–11539 (2008).
6. A. L. Oldenburg, J. R. Gunther, and S. A. Boppart, "Imaging magnetically labeled cells with magnetomotive optical coherence tomography," *Opt. Lett.* **30**(7), 747–749 (2005).
7. C. Wilhelm and F. Gazeau, "Universal cell labelling with anionic magnetic nanoparticles," *Biomaterials* **29**(22), 3161–3174 (2008).
8. C. K. Sung et al., "Dual-modal nanoprobes for imaging of mesenchymal stem cell transplant by MRI and fluorescence imaging," *Korean J. Radiol.* **10**(6), 613–622 (2009).
9. X. Liang et al., "Magnetomotive optical coherence microscopy for cell dynamics and biomechanics," *Proc. SPIE* **7889**, 788926–788927 (2011).
10. V. Crecea et al., "High resolution phase-sensitive magnetomotive optical coherence microscopy for tracking magnetic microbeads and cellular mechanics," *IEEE J. Sel. Top. Quantum Electron.* **20**(2), 25–31 (2014).
11. J. Koo et al., "Pulsed magneto-motive optical coherence tomography for remote cellular imaging," *Opt. Lett.* **37**(17), 3714–3716 (2012).
12. A. L. Oldenburg et al., "Magnetic and contrast properties of labeled platelets for magnetomotive optical coherence tomography," *Biophys. J.* **99**(7), 2374–2383 (2010).
13. A. L. Oldenburg et al., "Imaging and elastometry of blood clots using magnetomotive optical coherence tomography and labeled platelets," *IEEE J. Sel. Top. Quantum Electron.* **18**(3), 1100–1109 (2012).
14. A. L. Oldenburg et al., "Magnetic contrast agents for optical coherence tomography," *Proc. SPIE* **5316**, 91–98 (2004).
15. Y. Inoue et al., "Subretinal transplantation of bone marrow mesenchymal stem cells delays retinal degeneration in the RCS rat model of retinal degeneration," *Exp. Eye Res.* **85**(2), 234–241 (2007).
16. A. W. Joe and K. Gregory-Evans, "Mesenchymal stem cells and potential applications in treating ocular disease," *Curr. Eye Res.* **35**(11), 941–952 (2010).
17. T. V. Johnson et al., "Neuroprotective effects of intravitreal mesenchymal stem cell transplantation in experimental glaucoma," *Invest. Ophthalmol. Visual Sci.* **51**(4), 2051–2059 (2010).
18. B. Lu et al., "Human adult bone marrow-derived somatic cells rescue vision in a rodent model of retinal degeneration," *Exp. Eye Res.* **91**(3), 449–455 (2010).
19. A. Burkhardt et al., "Endoscopic optical coherence tomography device for forward imaging with broad field of view," *J. Biomed. Opt.* **17**(7), 071302 (2012).
20. R. John et al., "*In vivo* magnetomotive optical molecular imaging using targeted magnetic nanoprobes," *Proc. Natl. Acad. Sci. U. S. A.* **107**(18), 8085–8090 (2010).

21. Y. Hirakawa, T. Hasegawa, and T. Masujima, "Laser speckle microscope for instantaneous determination of condition of single living cell," *Jpn. J. Appl. Phys.* **44**(2), L85 (2005).
22. J. Walther and E. Koch, "Transverse motion as a source of noise and reduced correlation of the Doppler phase shift in spectral domain OCT," *Opt. Express* **17**(22), 19698–19713 (2009).
23. A. Yanai et al., "Focused magnetic stem cell targeting to the retina using superparamagnetic iron oxide nanoparticles," *Cell Transplant.* **21**(6), 1137–1148 (2012).
24. K. Franze et al., "Spatial mapping of the mechanical properties of the living retina using scanning force microscopy," *Soft Matter* **7**(7), 3147–3154 (2011).

Peter Cimalla is a postdoctoral research fellow in the workgroup Clinical Sensoring and Monitoring of professor Edmund Koch at the Technische Universität Dresden. He studied electrical and biomedical engineering and received his graduate engineer degree (Dipl.-Ing.) and doctoral degree (Dr.-Ing.) from the Faculty of Electrical and Computer Engineering at TU Dresden in 2007 and 2013, respectively. His current research interests include novel methods in optical coherence tomography and other optical imaging techniques for biomedical research.

Theresa Werner has studied physics at the University of Dresden since 2009. She wrote her bachelor's thesis in the workgroup Clinical Sensoring and Monitoring of professor Edmund Koch at the Technische Universität Dresden and received her BSc degree in 2013. Currently, she is writing her master's thesis about range verification in proton therapy at the National Center for Radiation Research in Oncology (OncoRay) in Dresden.

Kai Winkler studies biophysics in Berlin at Humboldt University. He received his BSc degree in physical engineering with special field medical technology, which he received in 2013 while working in the workgroup Clinical Sensoring and Monitoring of professor Edmund Koch at the Technische Universität Dresden.

Claudia Mueller studied biochemistry at the University of Leipzig and received her degree in 2008 (Dipl.-Biochemist). Since 2011, she has been working at the TU Dresden in the Institute of Anatomy. Currently, she works on the development of cell therapy for AMD (age-related macular degeneration) with human mesenchymal stem cells and on new methods to overcome rejection in cornea transplantation (silencing HLA expression in the cornea).

Sebastian Wicht is a PhD student at Technische Universität Dresden and works at the Leibniz Institute for Solid State and Materials Research Dresden e.V. (IFW Dresden). He holds a diploma (Dipl.-Ing.) in materials science that he earned from the Faculty of Materials Science and Engineering at the Technische Universität Dresden in 2012. His scientific interest and experience are focused on the structural and magnetic characterization of granular magnetic thin films used in data storage media.

Maria Gaertner started her research career in 2008 in the Biophysical Department (Schwille group) of the Technische Universität Dresden (TUD) by graduating in physics. Subsequently, she joined the Clinical Sensoring and Monitoring group of professor Edmund Koch at the TUD, receiving her PhD degree (Dr. rer. nat.) in 2013. Her current research interest comprises optical coherence tomography, fluorescence microscopy, spectroscopy, and optical tissue modeling for studies of lung-tissue dynamics as well as retinal degeneration processes.

Mirko Mehner is a research engineer in the workgroup Clinical Sensoring and Monitoring of professor Edmund Koch at the Technische Universität Dresden. He studied medical engineering and received his graduate engineer degree [Dipl.-Ing. (FH)] from the University of Applied Sciences Mittweida. His current research interests include optical measuring methods, measurement instrumentation (especially for blood pressure measurement), and other engineering methods of biomedical research. Additionally, he teaches medical physics for students of medicine and dentistry.

Julia Walther is a postdoctoral research fellow in the workgroup Clinical Sensoring and Monitoring of professor Edmund Koch at the Technische Universität Dresden. She studied physics engineering and received her graduate engineer degree [Dipl.-Ing. (FH)] from the University of Applied Sciences Mittweida and her doctoral degree (Dr. rer. medic.) from the TU Dresden, in 2006 and 2010, respectively. Her current research interests include precise velocity measurement using phase-resolved Doppler optical coherence tomography.

Bernd Rellinghaus received his PhD degree in physics from the University of Duisburg. Awarded with a research stipend of the German Science Foundation, he then joined the IBM Almaden Research Center in San Jose, California, USA. In 1997, he returned to Duisburg, and since 2004 has headed the Department for Metastable and Nanostructured Materials at the IFW Dresden. He is an expert in magnetic materials, transition metal alloys, nanoparticles (particularly nanomagnets), and high-resolution transmission electron microscopy.

Dierk Wittig is a physician at the Hospital of the Klinikum Chemnitz and a postdoctoral researcher in the group of Prof. Engelmann at TU Dresden. He studied medicine at the University Dresden and received his doctoral degree in basic science for his work in the field of cell communication in 2012. His current interests include the translation of basic research to a clinical application with a focus of retinal diseases and disorders.

Mike O. Karl is a research group leader at the DZNE and affiliated with the TU Dresden CRTD. The overall objectives are to find new ways to prevent retina degeneration and enable regeneration. Therefore, studies aim at deciphering mechanisms that control the fate of retinal cells throughout life. Current aims are to understand and overcome mechanisms limiting *de novo* neurogenesis (regeneration) in neurodegenerative diseases in mammals and the development of pluripotent stem cell-derived retina models for regenerative medicine.

Marius Ader heads the workgroup Cell Replacement in the Mammalian Retina at the Technische Universität Dresden. He studied biology followed by a PhD in neurobiology at ETH Zürich/Universities of Hamburg and Bielefeld. After a postdoc at Trinity College Dublin in 2007, he started his own research group at the CRTD, where he became a professor in 2014. He is developing cell-based therapies for degenerative retinal diseases by transplantation of photoreceptors and RPE cells.

Richard H. W. Funk got a professorship for anatomy in 1988 at the University Erlangen-Nürnberg with scientific focus on microscopy of blood vessels in the interactions with eye and retinal tissues. In 1994, he moved to the chair of anatomy, Medical Faculty, Technische Universität Dresden. He has concentrated his scientific work on microscopy immunohistochemistry and spectroscopy of different cell and tissue models for medical devices.

Edmund Koch received his PhD degree (Dr. rer. nat.) in 1984 at the Philipps-Universität Marburg. After a research period at the IBM Research Center in Yorktown Heights, USA, he joined the optical research group at Drägerwerk AG in 1986. In 1994, he became a professor of optics and lasers at the University of Applied Sciences in Lübeck. In 2003, he founded the research group Clinical Sensoring and Monitoring at the Medical Faculty of the TU Dresden.